A Geometric Interpretation of Reference Frames and Transformations: dq0, Clarke, and Park

A Geometric Interpretation of Reference Frames and Transformations: dq0, Clarke and Park

Colm J. O'Rourke, *Student Member, IEEE,* Mohammad M. Qasim, *Student Member, IEEE,*
Matthew R. Overlin, *Student Member, IEEE,* and James L. Kirtley Jr., *Life Fellow, IEEE*

***Abstract*—Transformations between abc, stationary dq0 ($\alpha\beta0$) and rotating dq0 reference-frames are used extensively in the analysis and control of three-phase technologies such as machines and inverters. Previous work on deriving the matrices describing these transformations follows one of two approaches. The first approach derives Clarke's matrix by modifying symmetrical components. Park's matrix can be subsequently found from a rotation matrix. The second approach derives Park's matrix using trigonometric projection by interpreting the transformation as a rotation in the plane of the cross-section of a machine. Then, Clarke's matrix can be found trivially using a reference angle of zero in Park's matrix. This paper presents a third approach to deriving the Clarke and Park transformation matrices: a geometric interpretation. The approach exploits properties of the linear transformation using the Cartesian representation. We introduce the locus diagram of a three-phase quantity and show how these diagrams have applications in power quality. We show that, unlike a phasor diagram, a single locus diagram can fully represent a three-phase system with harmonics.**

***Keywords*—dq0, Park, Clarke, reference-frame theory, locus diagram, power quality**

I. Introduction

TRANSFORMATIONS between abc and $dq0$ reference-frames were originally used to assist in electrical machine analysis and modelling [1]. Currently, $dq0$ based models are used in a wide variety of applications including: modelling and control of electric machines and drives [1], [2], multimachine modelling [3], multi-inverter modelling [4], microgrid simulation [5]–[7], phase-locked loops (PLLs) [8] and active power filters [9]. In many of these examples, the dq components no longer refer to the direct and quadrature axes of a machine. This motivates an alternative interpretation of reference-frames that is detached from any specific technology or application. This paper provides one such alternative perspective which we refer to as the "geometric interpretation".

Considering the wealth of literature available on the subject of reference frames, it is essential that this paper positions its contributions in the context of previous work. To this end, we must first study the history of these transformations, taking care to cite the most notable references. We review Krause's arbitrary reference-frame, and how this perspective relates to each transformation. Following this, we present the geometric approach to deriving the Clarke and Park transformation matrices. We distinguish the contributions of this paper from previous work, and the advantages and disadvantages of the geometric approach are discussed.

A. Review of the Clarke and Park Transformations

Fig. 1 provides an overview of the transformations. The Clarke transformation converts three-phase abc quantities to $\alpha\beta0$ (ie stationary $dq0$). The Park transformation converts abc quantities to $dq0$ and can be thought of as applying the Clarke transformation first, followed by the $\alpha\beta0$ to $dq0$ transformation. Here we refer to the latter as simply the "$dq0$ transformation" for simplicity of subscript notation. Later we will discuss how this corresponds to the "frame-to-frame-transformation" as described in [1].

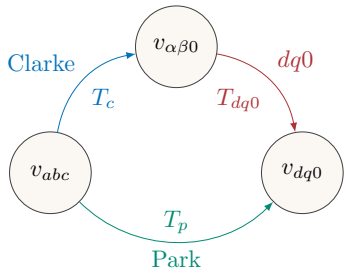

Fig. 1. Relationships between the Park and Clarke transformations. Note that the term "$dq0$ transform" as defined in this paper refers to a transformation from $\alpha\beta0$ to $dq0$ and is therefore not equivalent to the Park transformation.

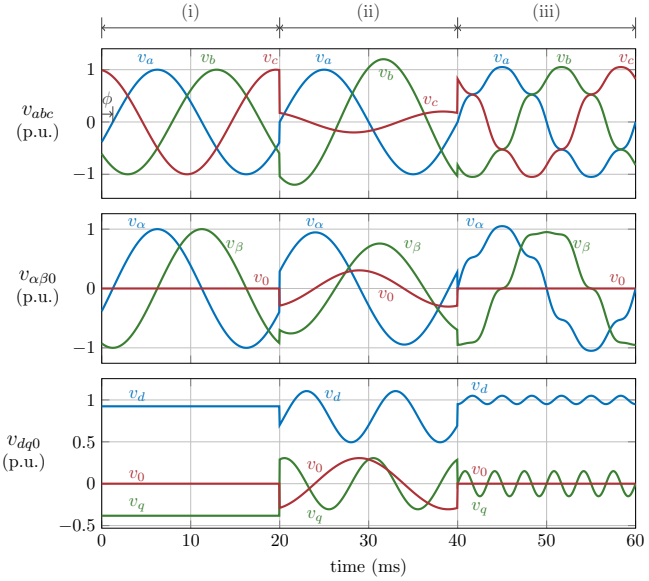

Fig. 2. Clarke and Park transformations applied to three-phase 50 Hz voltages 1 under three conditions: (i) balanced fundamental frequency with a phase shift (ii) unbalanced fundamental (iii) balanced with harmonics (1^{st}, 5^{th}, 7^{th}).

Fig. 2 shows the affect of applying the standard Clarke and Park transformations under three different conditions: (i) Balanced voltages result in equal magnitudes for v_α and v_β and constant values of v_d and v_q. (ii) Unbalanced voltages result in unequal magnitudes for v_α and v_β and time-varying v_d and v_q at the 2^{nd} harmonic. v_0 is a zero-sequence component at the fundamental and is always identical in both transformations.

Condition (iii) in Fig. 2 illustrates the affect of harmonics. Each phase voltage includes fundamental, 5^{th} and 7^{th} harmonics, with balanced voltages at each harmonic. These particular harmonics appear as a 6^{th} harmonic in v_d and v_q. There is no zero-sequence component for these particular harmonics. The voltage v_α is equivalent to v_a; and v_β has a different harmonic profile to v_b due to a 180° phase-shift on its positive sequence components. In Section V, each of the conditions (i), (ii) and (iii) in Fig. 2 are explained using the geometric interpretation.

1) History of the Clarke Transformation: In the 1930s, Clarke made a series of modifications to symmetrical components [10], [11]. These modifications simplified the calculations for certain classes of unbalanced three-phase problems [11], [12]. The α, β and 0 components were one set of these innovations [11], and were particularly useful as they did not require the $\underline{a}$ operator ($1\angle 120°$) or complex numbers.

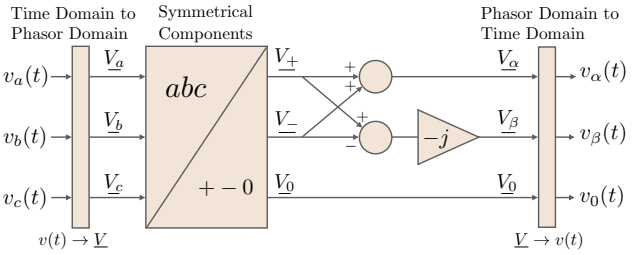

Fig. 3. An illustration of the Clarke transformation as derived in [11].

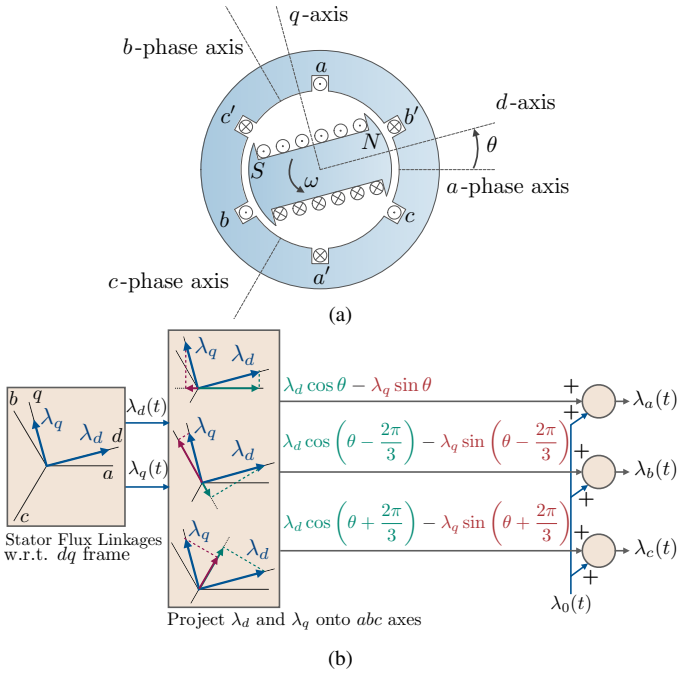

Fig. 4. An illustration of the Park transformation as derived in [13].
(a) Three-phase synchronous machine with magnetic axes labelled.
(b) Park's derivation of the inverse transformation.

Fig. 3 provides an illustration of the derivation developed by Clarke. The α component is defined as the sum of the positive and negative sequence voltage phasors, whereas the β component is the difference between positive and negative sequence phasors, times $-j$. Clarke's 0 component is equivalent to the zero sequence as defined by symmetrical components. For a comprehensive discussion of Clarke's derivation, we refer the reader to [11].

2) History of the Park Transformation: During the 1920s, Park generalised Blondel's Two-Reaction Theory of Synchronous Machines [13]–[16]. This method resolves the armature fluxes in a salient machine along the two axes of symmetry: the direct and quadrature axes. Fig. 4(a) shows the physical definitions of the direct and quadrature axes. Park's derivation shown in Fig. 4(b) actually defines the inverse transformation: $dq0$ to abc. The steps are as follows: Firstly, assume that armature flux linkages can be resolved into two components: directly in phase with the rotor (λ_d) and in quadrature with the rotor (λ_q). Secondly, project the d and q-axes flux linkages onto the three coplanar abc magnetic axes. Finally, add a zero sequence component (λ_0) to each phase. We refer the reader to [13] for a more complete description of Park's derivation.

B. Review of the Arbitrary Reference-Frame

A "reference-frame" refers to a set of $dq0$ axes rotating at a particular speed ω (which may be zero). In the 1920s Park chose to rotate his $dq0$ axes as defined in [13] at the rotor speed of a synchronous machine ω_r (because that speed eliminates time-varying inductance in synchronous machine analysis). During the 1930s-1950s others [17]–[19] used alternative reference speeds for their $dq0$ axes, to assist in the analysis of induction machines. Eliminating time-varying inductance in addition to achieving a diagonalised inductance matrix were primary objectives [1].

In 1965, Krause described in [20] that all of the different reference-frames used in [11], [13], [17]–[19] are specific applications of the "arbitrary reference-frame". They all refer to $dq0$ axes that rotate at a specified ω. A list of commonly used reference-frame speeds are given below [1]:

- ω. The $dq0$ axes rotate at an *arbitrary* speed. [20].
- $\omega = \omega_r$. The $dq0$ axes rotate at the *rotor* speed [13].
- $\omega = \omega_e$. The $dq0$ axes rotate at the *synchronous* speed.
- $\omega = 0$. The $dq0$ axes are *stationary* (Clarke transform).

All of the reference-frames listed can be described by Park's transformation matrix, except that each uses a different rotation speed ω for the $dq0$ axes. We refer the reader to [1] for an extensive discussion of the various reference-frames.

One of the goals of this work is to provide an alternative derivation of Park's transformation matrix, which describes all of the listed reference-frames (when the appropriate ω is inserted into this matrix). Therefore, we shall take a general approach and consider an arbitrary reference speed ω whenever we are referring to Park's transformation matrix. We will still refer to this matrix as "Park's transformation", even though we are not limiting the reference speed to be that of the rotor ω_r. One is free to choose any reference speed they wish.

C. Contributions

The contributions of this paper are summarised below. The remainder of this section elaborates on these points:

1) We group the previous approaches to deriving the matrices describing the Park and Clarke transformations into two approaches. This paper presents a third approach to deriving the Clarke and Park transformation matrices: a geometric approach.
2) We introduce the "locus diagram" of a three-phase quantity and how this locus changes in the presence of unbalance and harmonics.

The first contribution of this paper is to provide an alternative approach to derive the Park and Clarke transformations. Previous work on deriving these transformation matrices follows one of two approaches:

(i) The Clarke transformation matrix is derived from symmetrical components [11] as shown in Fig. 3. The Park transformation matrix can be subsequently derived using a rotation matrix such as Eq. (29).
(ii) The Park transformation matrix is derived trigonometrically by interpreting the transformation as a rotation in the plane of the cross-section of a machine. The abc axes are coplanar stationary axes that lie 120° apart and dq quantities can be projected onto the abc axes in a manner shown in Fig. 4(b). A third transformation variable is introduced to satisfy the change of variables. This is chosen to be the zero component, which is added separately. Many authors trigonometrically project in the opposite manner: from abc to dq and are thus required to specify scaling factors k_d and k_q, normally equal to either $2/3$ or $\sqrt{2/3}$: see [21]. These projections describe the approach taken by the majority of authors such as [1], [13], [17]–[24]. The Clarke transformation matrix can then be derived trivially by setting $\omega = 0$ in Park's transformation matrix. One should note that the coplanar abc axes are usually considered to have a physical meaning relating to the magnetic axes in the cross-section of a machine as in Fig. 4(a), but this

physical interpretation of the abc axes is not necessary to derive the matrix [1].

This paper presents a third approach to deriving the Clarke and Park transformation matrices: a geometric interpretation. This geometric approach uses the Cartesian representation: three-phase quantities are represented by vectors in $\mathbb{R}^3$, where each orthogonal component of the vector corresponds to the instantaneous value of one of the three phases. The first appearance of the Cartesian representation applied to three-phase quantities was given by Lipo in [25]. Other work that uses this representation includes [26], [27]. More recently, Montanari and Gole use a three-dimensional perspective to introduce a new transformation termed the "mno-transform" [28]. The mno-transformation assists in the calculation of instantaneous real and reactive power for systems containing four-wire inverters. This enables the mitigation of power oscillations that normally occur when such systems are unbalanced [28]. Although others have utilised the Cartesian representation in [25]–[28], this paper is unique as the representation is used to derive the matrices describing the Clarke and Park transformations.

The geometric approach is explained step-by-step in Section III and Section IV. A summary of the derivations provided by the geometric view is given by Fig. 5. Each transformation is interpreted as a combination of vector rotation and scaling in $\mathbb{R}^3$. The abc axes are orthogonal stationary axes that lie 90° apart and have basis vectors that span $\mathbb{R}^3$. We exploit the linearity property of matrix transformations, and derive each transformation matrix by observing how each transformation affects the orthonormal basis vectors of the vector space.

The geometric approach has many advantages when compared to the two traditional approaches listed previously. These include:

- When trigonometrically deriving the Park transformation such as in Fig. 4(b), zero-sequence components are treated separately in the derivation. The d and q components are found from a projection operation whereas the 0 components are added separately. The geometric approach finds all $dq0$ components in a unified manner via Eq. (4).
- The previous approaches interpret the Clarke transformation as either a manipulation of symmetrical components as in Fig. 3, or as a specialised case of the arbitrary reference-frame with stationary $dq0$ axes [1]. The geometric approach interprets the power-invariant Clarke transformation as a single rotation in $\mathbb{R}^3$, which some readers may find to be a simpler explanation (see Fig. 8). The standard (amplitude-invariant) Clarke transformation is shown in Fig. 10 to be a combination of rotation and scaling in $\mathbb{R}^3$.
- Similarly, previous approaches interpret the Park transformation as either a manipulation of symmetrical components [11] combined with a rotation matrix, or as a projection onto coplanar abc axes [13]. The geometric approach interprets the power-invariant Park transformation as two consecutive rotations in $\mathbb{R}^3$, which some readers may find to be more intuitive (see Fig. 5). The standard Park transformation is interpreted as first applying the standard Clarke transform (rotation and scaling) followed by a pure rotation in $\mathbb{R}^3$ given by Fig. 12.
- The orthogonality ($\boldsymbol{A}^\intercal = \boldsymbol{A}^{-1}$) of the power-invariant forms of both transformations can be easily seen from all three approaches via matrix manipulation. The geometric interpretation illustrates this orthogonal property: orthogonal transformations preserve vector length and can thus be visualised as pure rotations in $\mathbb{R}^3$ [29].

The disadvantages of the geometric interpretation, compared with the two traditional approaches include:

- The geometric derivation is more involved. This can be seen by comparing Fig. 5 to the two traditional approaches illustrated by Fig. 3 and Fig. 4(b).
- The diagrams required to explain the geometric view are more complex to draw as they are three-dimensional.

The second contribution of this paper involves the "locus diagram" of a three-phase quantity and how this locus changes in the presence of unbalance and harmonics. This contribution consists of the following:

- In Section II-C we show that for balanced systems, the locus corresponds to a circle in $\mathbb{R}^3$. We derive Eq. (12) which shows that this circle has a radius of $V\sqrt{3/2}$ where V is the voltage magnitude on each phase.
- In Section V we extend the locus diagram to cases of harmonics and unbalance. Systems with purely positive and negative sequence will have a locus that lies within the $\alpha\beta$-plane. The locus of a zero-sequence component is a line segment perpendicular to the $\alpha\beta$-plane.
- We show that a single locus diagram can fully represent a three-phase quantity containing harmonics in Fig. 18. This is not possible using a single phasor diagram.

II. Transformations, Cartesian Representations & The Locus of Three-Phase Quantities

This section introduces the mathematical tools that are used to develop geometric derivations of the Clarke and Park transformation matrices. Firstly, we review the fundamentals of linear transformations. Secondly, we describe the Cartesian representation and compare it with phasor notation. Thirdly, we introduce the concept of the *locus* of a three-phase quantity, and show that the locus of a balanced set of signals is a circle in $\mathbb{R}^3$.

A. Review of Linear Transformations

Transformations are functions that operate on vectors. This section derives a basic method to finding a unique matrix $\boldsymbol{A}$ that fully describes a linear transformation $T\colon \mathbb{R}^n \to \mathbb{R}^m$.

Any vector $\vec{v} \in \mathbb{R}^n$ can be written as a linear combination of the standard basis unit vectors $\{\hat{\mathbf{e}}_1, \hat{\mathbf{e}}_2, \ldots, \hat{\mathbf{e}}_n\}$.

$$\vec{v} = v_1\hat{\mathbf{e}}_1 + v_2\hat{\mathbf{e}}_2 + \ldots + v_n\hat{\mathbf{e}}_n \tag{1}$$

To find $T(\vec{v}) \in \mathbb{R}^m$ we apply the linear transformation T to $\vec{v}$ and impose the additivity and homogeneity constraints of linearity:

$$T(\vec{v}) = v_1T(\hat{\mathbf{e}}_1) + v_2T(\hat{\mathbf{e}}_2) + \ldots + v_nT(\hat{\mathbf{e}}_n) \tag{2}$$

$T(\vec{v})$ in Eq. (2) is now expressed in terms of transformed standard basis vectors scaled by the components of $\vec{v}$. Such a linear combination of column vectors can always be written as a matrix-vector product:

$$T(\vec{v}) = \begin{bmatrix} | & | & & | \\ T(\hat{\mathbf{e}}_1) & T(\hat{\mathbf{e}}_2) & \ldots & T(\hat{\mathbf{e}}_n) \\ | & | & & | \end{bmatrix} \begin{bmatrix} v_1 \\ v_2 \\ \vdots \\ v_n \end{bmatrix}$$

$$T(\vec{v}) = \boldsymbol{A}\vec{v} \tag{3}$$

Eq. (3) says that any linear transformation $T\colon \mathbb{R}^n \to \mathbb{R}^m$ can be expressed as a matrix-vector product $\boldsymbol{A}\vec{v}$.

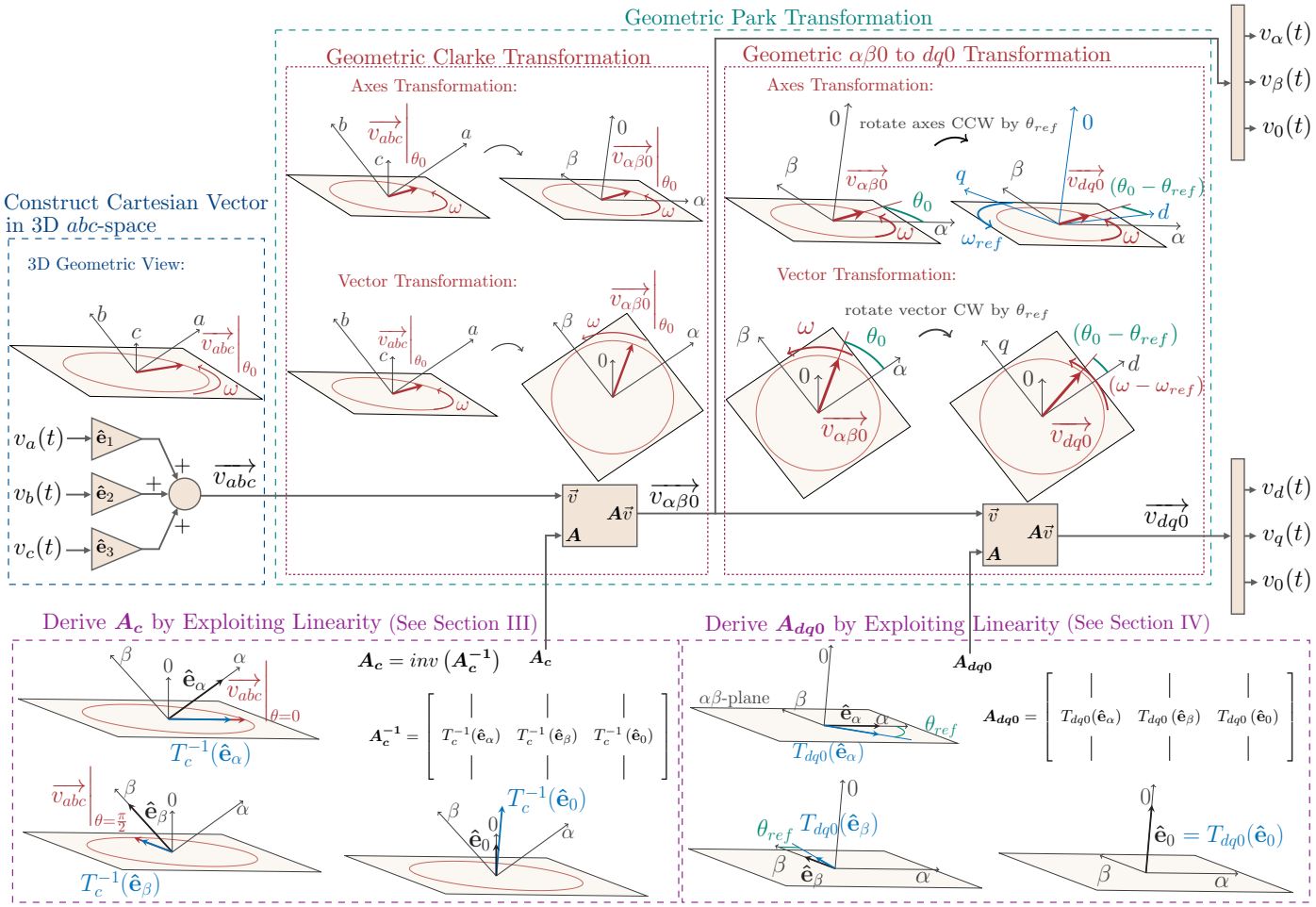

Fig. 5. Geometric interpretation of the Clarke and Park transformations.

$$\boldsymbol{A} = \begin{bmatrix} | & | & & | \\ T(\hat{\mathbf{e}}_1) & T(\hat{\mathbf{e}}_2) & \dots & T(\hat{\mathbf{e}}_n) \\ | & | & & | \end{bmatrix} \tag{4}$$

Eq. (4) describes a technique to determine the $m \times n$ matrix $\boldsymbol{A}$, that corresponds to the linear transformation $T\colon \mathbb{R}^n \to \mathbb{R}^m$. We can construct $\boldsymbol{A}$ by applying the linear transformation to each of the basis vectors of $\mathbb{R}^n$. We shall use Eq. (4) to geometrically derive the Park and Clarke transformation matrices $\boldsymbol{A}_P$ and $\boldsymbol{A}_C$.

B. Cartesian Representation of Three-Phase Voltages

Three-phase quantities such as voltages, currents and flux linkages are often expressed using phasor notation. This section introduces the Cartesian representation and compares it with phasor notation.

1) Phasor Representation: Eq. (5) is an example of a set of three-phase voltages with no harmonics. For now these voltages may or may not be balanced, where "balanced" would require $\phi_a = \phi_b = \phi_c = 0$ and $V_a = V_b = V_c$.

$$\begin{cases} v_a(t) = V_a \cos(\omega t + \phi_a) \\ v_b(t) = V_b \cos(\omega t - \frac{2\pi}{3} + \phi_b) \\ v_c(t) = V_c \cos(\omega t + \frac{2\pi}{3} + \phi_c) \end{cases} \tag{5}$$

Each of the three sinusoidal voltages in Eq. (5) can be represented by a unique phasor. Phasor notation is the use of a single complex known as a *phasor* to store the two parameters of magnitude V and phase ϕ. The magnitude of the phasor $\underline{V_i}$ represents the RMS value of $v_i(t)$ and the phase ϕ_i corresponds to the angle of the voltage $v_i(t)$.

Note that the expression for each sinusoidal voltage in Eq. (5) is actually defined by three parameters: voltage magnitude V_i, phase ϕ_i and frequency ω. A known frequency must be assumed, which is one limitation of the phasor representation. In addition, the phasor representation cannot be used to represent signals containing more than one frequency component, such as signals with harmonics.

Eq. (6) expresses the voltages in Eq. (5) as three phasors $\underline{V_a}, \underline{V_b}$ and $\underline{V_c}$. These three phasors can be drawn on a single complex plane in a phasor diagram. Fig. 6(a) draws a balanced case.

$$\begin{cases} \underline{V_a} = \frac{1}{\sqrt{2}} V_a e^{j\phi_a} \\ \underline{V_b} = \frac{1}{\sqrt{2}} V_b e^{j\left(-\frac{2\pi}{3} + \phi_b\right)} \\ \underline{V_c} = \frac{1}{\sqrt{2}} V_c e^{j\left(\frac{2\pi}{3} + \phi_c\right)} \end{cases} \tag{6}$$

Each voltage phasor in Eq. (6) can be converted back to a function of time using Euler's relation as shown in Eq. (7).

$$v_i(t) = \sqrt{2}\,\mathrm{Re}\{\underline{V_i} e^{j\omega t}\} \tag{7}$$

2) Cartesian Representation: We use the notation $\overrightarrow{v_{abc}}$ to signify the Cartesian representation of a set of three-phase voltages. Previous work that uses the Cartesian representation applied to three phase quantities includes: [25]–[28]. $\overrightarrow{v_{abc}}$ is a single vector in $\mathbb{R}^3$ and has three components corresponding to three orthogonal abc axes:

$$\overrightarrow{v_{abc}} = v_a \hat{\mathbf{e}}_a + v_b \hat{\mathbf{e}}_b + v_c \hat{\mathbf{e}}_c \tag{8}$$

The components of Eq. (8) vary with time. Thus $\overrightarrow{v_{abc}}$ is a vector that moves in $\mathbb{R}^3$ over time as seen in Eq. (9):

$$\overrightarrow{v_{abc}}(t) = \begin{bmatrix} v_a(t) \\ v_b(t) \\ v_c(t) \end{bmatrix} = \begin{bmatrix} V_a \cos(\omega t + \phi_a) \\ V_b \cos(\omega t - \frac{2\pi}{3} + \phi_b) \\ V_c \cos(\omega t + \frac{2\pi}{3} + \phi_c) \end{bmatrix} \tag{9}$$

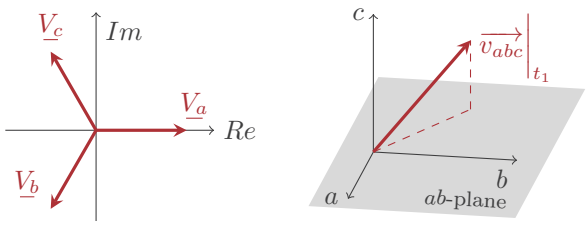

(a) (b)

Fig. 6. Three-phase voltage representations: (a) Phasor representation (b) Cartesian representation at time t_1.

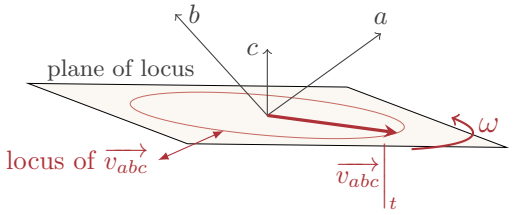

Fig. 7. Locus diagram of balanced three-phase voltages.

Fig. 6(b) plots $\overrightarrow{v_{abc}}(t)$ at a particular instance in time t_1. We will see later that the *locus* traced out by $\overrightarrow{v_{abc}}(t)$ over one period is of particular interest.

Fig. 6 compares the phasor and Cartesian representations for a three-phase system.

- Phasor Representation:
  - $\mathbb{C}$ vector space with two axes Re and Im.
  - Three complex numbers (phasors) $\underline{V}_a, \underline{V}_b$ and $\underline{V}_c$ that do not vary with time.
- Cartesian Representation:
  - $\mathbb{R}^3$ vector space with three orthoganal axes a, b, c.
  - Single vector $\overrightarrow{v_{abc}}$ that moves with time.

C. The Locus of Balanced Three-Phase Voltages

The locus diagram is a complete graphical representation of a three-phase quantity. Whereas the phasor diagram of Fig. 6(a) cannot represent signals with more than one frequency component; the locus diagram can represent both harmonics and unbalance at each harmonic (See Section V for locus diagrams with harmonics and unbalance).

Fig. 7 is an example of a locus diagram. The voltages are defined by Eq. (9) for the balanced case, with peak magnitudes $V_a = V_b = V_c = V$ and $\phi_a = \phi_b = \phi_c$. The vector $\overrightarrow{v_{abc}}$ moves in $\mathbb{R}^3$ with time. This can be seen by examining how the orthogonal components of $\overrightarrow{v_{abc}}$ in Eq. (9) vary with time.

We define the locus as the path in $\mathbb{R}^3$ that $\overrightarrow{v_{abc}}$ traverses over one cycle of the lowest frequency component. Fig. 7 shows that the locus of $\overrightarrow{v_{abc}}$ traces out a circle in $\mathbb{R}^3$ for a balanced set of three-phase voltages that contain no harmonics. $\overrightarrow{v_{abc}}$ rotates at a frequency of ω about this circle.

The circular nature of the locus of balanced voltages may not be obvious at first, so we shall show this algebraically. If the length of the vector $\overrightarrow{v_{abc}}$ is constant for all of time, then the locus must trace out a circle. The euclidean distance in $\mathbb{R}^3$ is given by:

$$\|\overrightarrow{v_{abc}}(t)\| = \sqrt{v_a(t)^2 + v_b(t)^2 + v_c(t)^2} \tag{10}$$

Assuming balanced voltages with each phase having a peak magnitude of V, and each with a phase angle $\phi = 0$, we can rewrite Eq. (10) using Eq. (9) to give:

$$\|\overrightarrow{v_{abc}}(t)\| = V\left[\cos^2(\omega t) + \cos^2\left(\omega t - \frac{2\pi}{3}\right) + \cos^2\left(\omega t + \frac{2\pi}{3}\right)\right]^{1/2} \tag{11}$$

Eq. (11) can be rewritten using trigonometric identities to give:

$$\|\overrightarrow{v_{abc}}(t)\| = V\sqrt{\frac{3}{2}\sin^2(\omega t) + \frac{3}{2}\cos^2(\omega t)}$$

$$\|\overrightarrow{v_{abc}}(t)\| = V\sqrt{\frac{3}{2}} \quad \forall\ t \tag{12}$$

Eq. (12) shows that the locus of $\overrightarrow{v_{abc}}$ is a circle in $\mathbb{R}^3$ for a balanced set of three-phase voltages, as the vector length is constant. This circle is shown in Fig. 7 and has a radius of $V\sqrt{3/2}$ where V is the voltage magnitude on each phase.

This exercise of finding the length of $\overrightarrow{v_{abc}}$ also illustrates another important concept: the length of $\overrightarrow{v_{abc}}$ is not equivalent to the peak phase voltage, even when the voltages are balanced. It is scaled by $\sqrt{3/2}$. This geometric analysis explains why the power-invariant Clarke and Park transformations have such scaling terms, as will be discussed in sections III and IV.

III. Geometric Derivation of the Clarke Transformation

There are two versions of the Clarke transformation: the standard (amplitude-invariant) transformation and the power-invariant transformation. The derivation introduced by Clarke as shown in Fig. 3 is the amplitude-invariant form, which is the most commonly used version. It is convenient because the magnitude of v_α is the same as the magnitude of v_a when the voltages are balanced. Previous approaches to deriving the Clarke transformation either rely on a manipulation of symmetrical components [11], or use the arbitrary reference-frame with stationary axes [1]. In this section, we use the geometric approach to derive both the standard and power-invariant Clarke transformations. The power-invariant version is derived first, as it is geometrically simpler.

A. Power-Invariant Clarke Transformation Derivation

The power-invariant Clarke transformation is a pure rotation, such that the locus of a balanced three-phase quantity lies in the ab-plane. Fig. 8 illustrates the locus diagrams for the geometric power-invariant Clarke transformation.

All transformations can be visualised as either a coordinate (axes) transformation or as a vector transformation. Fig. 8(a) is the axes transformation where the vector is fixed and the abc axes are rotated such that the locus of a balanced system lies in the rotated ab-plane (ie the $\alpha\beta$-plane). Fig. 8(b) is the vector transformation, where the axes are fixed and the vector rotates such that its locus lies in the ab-plane.

Note that there are infinite transformations that can achieve a locus that lies in the ab-plane, but only one of these anchor the α-axis so that it is in line with the balanced Cartesian voltage when the phase angle is zero ($\theta = \omega t + \phi = 0$), as seen in Fig. 8 . We will see later that this family of infinite transformations is given by Park's matrix where substituting a value of theta anchors the α-axis at a different location in the plane.

Using the constraints of bringing the locus into the ab-plane and anchoring the α-axis appropriately we can determine the matrix associated with the power-invariant Clarke transformation. In Section II-A we derived Eq. (4) which describes steps to find a matrix (e.g. $\boldsymbol{A_c}$) that represents a linear transformation (T_c). These steps require one to know how each orthonormal basis vector of a given space is affected by a transformation.

The inverse Clarke transformation T_c^{-1} is more convenient to derive geometrically than T_c. One can visualise how T_c^{-1} transforms vectors by reading Fig. 8 from right to left. The inverse transformation rotates the unit vectors $\hat{\mathbf{e}}_\alpha$ and $\hat{\mathbf{e}}_\beta$ such that they lie in the plane of $\overrightarrow{v_{abc}}$. Thus, these transformed unit

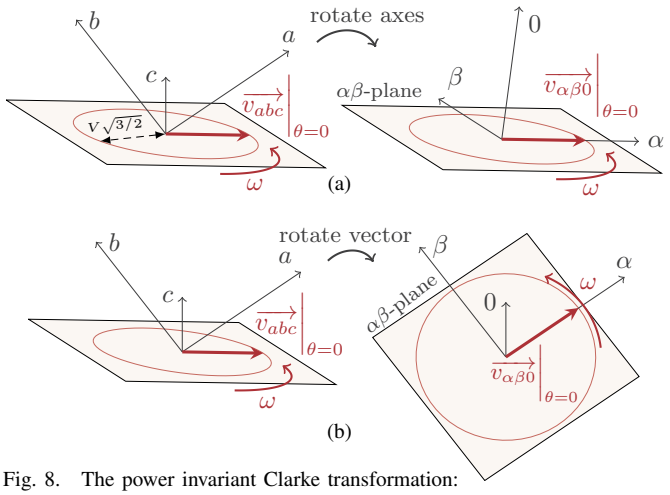

Fig. 8. The power invariant Clarke transformation:
(a) Axes transformation perspective: rotate the abc-axes such that the a-axis lines up with the vector v_{abc} at $\theta = 0$, and the b-axis also lies in the rotated ab-plane ($\alpha\beta$-plane). The rotated ab-axes become our $\alpha\beta$-axes respectively. The rotated c-axis becomes our 0-axis.
(b) Vector transformation perspective: rotate the voltage vector v_{abc} such that its locus lies in the ab-plane.

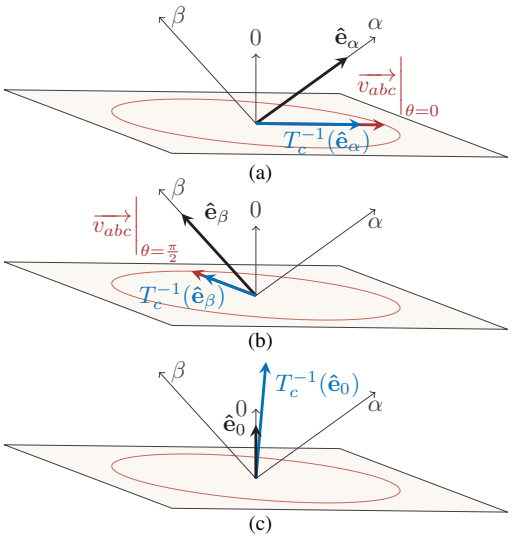

Fig. 9. Geometric power-invariant inverse Clarke derivation:
(a) rotate $\hat{\mathbf{e}}_\alpha$ to align with the vector v_{abc} at $\theta = 0$
(b) rotate $\hat{\mathbf{e}}_\beta$ to align with the vector v_{abc} at $\theta = \pi/2$
(c) rotate $\hat{\mathbf{e}}_0$ perpendicular to the plane.
Note: This figure uses the vector transformation perspective shown in Fig. 8(b). This perspective highlights how the unit vectors rotate, which allows us to evaluate Eq. (14)

vectors $T_c^{-1}(\hat{\mathbf{e}}_\alpha), T_c^{-1}(\hat{\mathbf{e}}_\beta)$ have a direction given by $\overrightarrow{v_{abc}}$ at angles of $\theta = 0$ and $\theta = \pi/2$ respectively. Whereas T_c rotates the abc unit vectors $\hat{\mathbf{e}}_a, \hat{\mathbf{e}}_b, \hat{\mathbf{e}}_c$ to a location that is inconvenient to determine.

$$\overrightarrow{v_{abc}} = T_c^{-1}\left(\overrightarrow{v_{\alpha\beta 0}}\right) = \boldsymbol{A_c^{-1}}\overrightarrow{v_{\alpha\beta 0}} \tag{13}$$

The matrix $\boldsymbol{A_c^{-1}}$ in Eq. (13) can be rewritten using Eq. (4):

$$\boldsymbol{A_c^{-1}} = \begin{bmatrix} | & | & | \\ T_c^{-1}(\hat{\mathbf{e}}_\alpha) & T_c^{-1}(\hat{\mathbf{e}}_\beta) & T_c^{-1}(\hat{\mathbf{e}}_0) \\ | & | & | \end{bmatrix} \tag{14}$$

These three steps of Eq. (14) are shown graphically in Fig. 9. Each step involves a rotation of a unit vector. We apply the inverse power-invariant Clarke transformation T_c^{-1} to each of the three $\alpha\beta 0$ unit vectors $\{\hat{\mathbf{e}}_\alpha, \hat{\mathbf{e}}_\beta, \hat{\mathbf{e}}_0\}$. Fig. 9(a) shows how $\hat{\mathbf{e}}_\alpha$ is transformed under the inverse power-invariant Clarke transformation. Its transformed direction is given by the Cartesian voltage when the angle is zero:

$$T_c^{-1}(\hat{\mathbf{e}}_\alpha) = \frac{\overrightarrow{v_{abc}}\big|_{\theta=0}}{\|\overrightarrow{v_{abc}}\|} \tag{15}$$

We showed in Section II-C that balanced three-phase systems have circular loci with a radius given by Eq. (12). Substituting Eq. (12) into Eq. (15) gives:

$$T_c^{-1}(\hat{\mathbf{e}}_\alpha) = \frac{1}{V}\sqrt{\frac{2}{3}}\,\overrightarrow{v_{abc}}\Big|_{\theta=0} = \sqrt{\frac{2}{3}}\begin{bmatrix} \cos\theta \\ \cos\left(\theta - \frac{2\pi}{3}\right) \\ \cos\left(\theta + \frac{2\pi}{3}\right) \end{bmatrix}\Big|_{\theta=0} \tag{16}$$

We then evaluate $\overrightarrow{v_{abc}}$ when the angle is zero:

$$T_c^{-1}(\hat{\mathbf{e}}_\alpha) = \sqrt{\frac{2}{3}}\begin{bmatrix} 1 & -\frac{1}{2} & -\frac{1}{2} \end{bmatrix}^\mathsf{T} \tag{17}$$

Fig. 9(b) illustrates how the the unit vector $\hat{\mathbf{e}}_\beta$ is rotated to align with the Cartesian voltage when the angle is $\pi/2$.

$$T_c^{-1}(\hat{\mathbf{e}}_\beta) = \frac{\overrightarrow{v_{abc}}\big|_{\theta=\frac{\pi}{2}}}{\|\overrightarrow{v_{abc}}\|}$$

$$T_c^{-1}(\hat{\mathbf{e}}_\beta) = \frac{1}{V}\sqrt{\frac{2}{3}}\,\overrightarrow{v_{abc}}\Big|_{\theta=\frac{\pi}{2}} = \sqrt{\frac{2}{3}}\begin{bmatrix} 0 & \frac{\sqrt{3}}{2} & -\frac{\sqrt{3}}{2} \end{bmatrix}^\mathsf{T} \tag{18}$$

In Fig. 9(c) we see how $\hat{\mathbf{e}}_0$ is rotated such that it is perpendicular to the plane of a balanced locus. Mathematically, this can be thought of as pointing in the direction of the cross product of $\hat{\mathbf{e}}_\alpha$ and $\hat{\mathbf{e}}_\beta$, as given by the right-hand rule:

$$T_c^{-1}(\hat{\mathbf{e}}_0) = \frac{\overrightarrow{v_{abc}}\big|_{\theta=0} \times \overrightarrow{v_{abc}}\big|_{\theta=\frac{\pi}{2}}}{\left\|\overrightarrow{v_{abc}}\big|_{\theta=0} \times \overrightarrow{v_{abc}}\big|_{\theta=\frac{\pi}{2}}\right\|}$$

$$T_c^{-1}(\hat{\mathbf{e}}_0) = \sqrt{\frac{2}{3}}\begin{bmatrix} \frac{1}{\sqrt{2}} & \frac{1}{\sqrt{2}} & \frac{1}{\sqrt{2}} \end{bmatrix}^\mathsf{T} \tag{19}$$

The three steps given by Eq. (17), Eq. (18) and Eq. (19) are combined with Eq. (14) to find $\boldsymbol{A_c^{-1}}$.

$$\boldsymbol{A_c^{-1}} = \sqrt{\frac{2}{3}}\begin{bmatrix} 1 & 0 & \frac{1}{\sqrt{2}} \\ -\frac{1}{2} & \frac{\sqrt{3}}{2} & \frac{1}{\sqrt{2}} \\ -\frac{1}{2} & -\frac{\sqrt{3}}{2} & \frac{1}{\sqrt{2}} \end{bmatrix} \tag{20}$$

The matrix $\boldsymbol{A_c^{-1}}$ is an orthogonal matrix because it is associated with a pure rotation. This means its transpose is equal to its inverse, $\boldsymbol{A_c} = \left(\boldsymbol{A_c^{-1}}\right)^\mathsf{T}$.

B. Standard Clarke Transformation Derivation

The standard (amplitude-invariant) Clarke transformation was originally derived by Clarke in a manner shown in Fig. 3. This section geometrically derives the amplitude-invariant Clarke transformation which has become the standard version.

The standard Clarke transformation is a rotation and scaling, such that the locus of a balanced three-phase quantity lies in the ab-plane with a radius equal to the phase magnitude. It can be thought of as first applying the pure rotation described by the power-invariant Clarke transformation followed by a scaling operation. Eq. (12) shows that the locus of a balanced three-phase voltage is a circle of radius $V\sqrt{3/2}$. The standard Clarke transformation scales this locus, such that the circle has a radius of V.

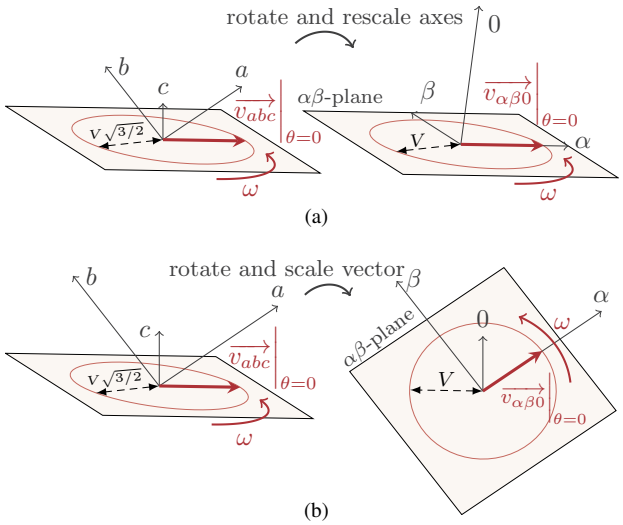

Fig. 10. The standard (amplitude-invariant) Clarke transformation:
(a) Axes transformation perspective: rotate the abc-axes such that the a-axis lines up with the vector v_{abc} at $\theta = 0$, and the b-axis also lies in the plane. Stretch the rotated ab-axes by $\sqrt{3/2}$ such that the circle traced by $v_{\alpha\beta 0}$ has a radius of V, when referenced to the $\alpha\beta$-axes. The rotated and stretched ab-axes become our $\alpha\beta$-axes respectively. The rotated c-axis becomes our 0-axis, and is stretched by $\sqrt{3}$ in order to agree with the definition of zero-sequence.
(b) Vector transformation perspective: rotate the vector v_{abc} such that it lies in the ab-plane. Scale the rotated v_{abc} by $\sqrt{2/3}$ such that it has a length of V when referenced to the $\alpha\beta$-plane. The 0-component of the vector $v_{\alpha\beta 0}$ is scaled by $1/\sqrt{3}$ in order to agree with the definition of zero-sequence.

Fig. 10 illustrates the locus diagrams for the geometric amplitude-invariant Clarke transformation. Fig. 10(a) is the axes transformation where the vector is fixed and the abc axes are rotated such that the locus of a balanced system lies in the $\alpha\beta$-plane. The α and β axes are stretched by $\sqrt{3/2}$ such that the locus traced by a balanced voltage has a radius equal to V, the peak magnitude of the phase voltage. The 0-axis is stretched by $\sqrt{3}$ making this equivalent to the symmetrical components definition of zero-sequence. Whatever voltage exists on the 0-axis will appear with the same magnitude on the a, b and c axes.

Fig. 10(b) is the vector transformation, where the axes are fixed and the vector rotates such that its locus lies in the ab-plane. The vector's α and β components are scaled by $\sqrt{2/3}$, meaning the locus of a balanced Cartesian vector will appear as a circle with a radius of V when referenced to the $\alpha\beta 0$ axes. The 0-axis is scaled by $1/\sqrt{3}$ to match the symmetrical components definition of zero-sequence.

Just as with the power-invariant transformation, there are infinite transformations that can achieve a locus that lies in the ab-plane with the scaling described as above. However, only one of these ensure that the α-axis is in line with the balanced Cartesian voltage when the phase angle is zero ($\theta = \omega t + \phi = 0$).

We follow the same procedure as the power-invariant derivation. Once again, we find the matrix $\boldsymbol{A_c^{-1}}$ associated with the inverse transformation T_c^{-1} using Eq. (14). Please refer to Section III-A for a discussion on why we choose to derive the inverse Clarke transformation.

The three steps described by Eq. (14) are shown graphically in Fig. 11. They involve transforming each of the three unit vectors under T_c^{-1}. Fig. 11(a) shows how $\hat{\mathbf{e}}_\alpha$ is transformed under the inverse standard Clarke transformation. $\hat{\mathbf{e}}_\alpha$ is rotated and stretched by $\sqrt{3/2}$, making it equivalent to the per-unit Cartesian voltage when the angle is zero.

$$T_c^{-1}(\hat{\mathbf{e}}_\alpha) = \overrightarrow{v_{abc}}\Big|_{\substack{V=1\\ \theta=0}} = \begin{bmatrix} V\cos\theta \\ V\cos\left(\theta - \frac{2\pi}{3}\right) \\ V\cos\left(\theta + \frac{2\pi}{3}\right) \end{bmatrix}\Bigg|_{\substack{V=1\\ \theta=0}}$$

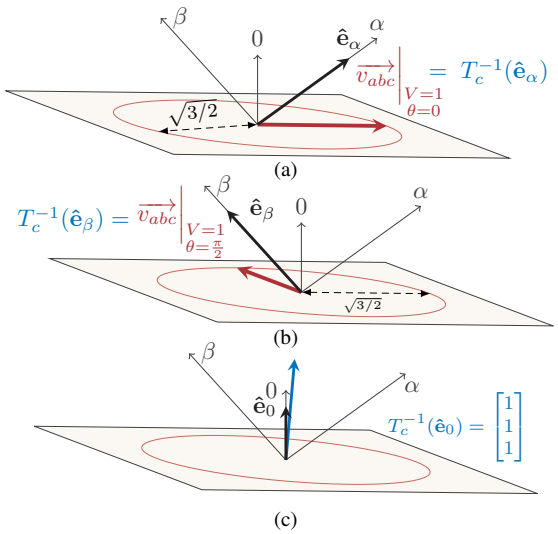

Fig. 11. Geometric standard (amplitude-invariant) inverse Clarke derivation:
(a) rotate $\hat{\mathbf{e}}_\alpha$ to align with the vector v_{abc} at $\theta = 0$ and stretch by $\sqrt{3/2}$
(b) rotate $\hat{\mathbf{e}}_\beta$ to align with the vector v_{abc} at $\theta = \frac{\pi}{2}$ and stretch by $\sqrt{3/2}$
(c) rotate $\hat{\mathbf{e}}_0$ perpendicular to the plane and stretch by $\sqrt{3}$.
Note: This figure uses the vector transformation perspective shown in Fig. 10(b). This perspective highlights how the unit vectors stretch and rotate, which allows us to evaluate Eq. (14)

$$T_c^{-1}(\hat{\mathbf{e}}_\alpha) = \begin{bmatrix} 1 & -\frac{1}{2} & -\frac{1}{2} \end{bmatrix}^\intercal \tag{21}$$

Similarly, Fig. 11(b) shows that $\hat{\mathbf{e}}_\beta$ is rotated and stretched by $\sqrt{3/2}$, making it equivalent to the per-unit Cartesian voltage when the angle is $\pi/2$.

$$T_c^{-1}(\hat{\mathbf{e}}_\beta) = \overrightarrow{v_{abc}}\Big|_{\substack{V=1\\ \theta=\frac{\pi}{2}}} = \begin{bmatrix} 0 & \frac{\sqrt{3}}{2} & -\frac{\sqrt{3}}{2} \end{bmatrix}^\intercal \tag{22}$$

Fig. 11(c) explains how $\hat{\mathbf{e}}_0$ is transformed. It points perpendicular to the plane in which the locus of $\overrightarrow{v_{abc}}$ lies, and is scaled by $\sqrt{3}$. The scaling is necessary so that the 0-component agrees with the 0-sequence as defined by symmetrical components.

$$T_c^{-1}(\hat{\mathbf{e}}_0) = \sqrt{3}\,\frac{\overrightarrow{v_{abc}}\Big|_{\theta=0} \times \overrightarrow{v_{abc}}\Big|_{\theta=\frac{\pi}{2}}}{\left\|\overrightarrow{v_{abc}}\Big|_{\theta=0} \times \overrightarrow{v_{abc}}\Big|_{\theta=\frac{\pi}{2}}\right\|} = \begin{bmatrix}1\\1\\1\end{bmatrix} \tag{23}$$

The three transformed unit vectors given by Eq. (21), Eq. (22) and Eq. (23) are combined with Eq. (14) to find $\boldsymbol{A_c^{-1}}$.

$$\boldsymbol{A_c^{-1}} = \begin{bmatrix} 1 & 0 & 1 \\ -\frac{1}{2} & \frac{\sqrt{3}}{2} & 1 \\ -\frac{1}{2} & -\frac{\sqrt{3}}{2} & 1 \end{bmatrix} \tag{24}$$

We find $\boldsymbol{A_c}$ by taking the inverse of the matrix $\boldsymbol{A_c^{-1}}$.

IV. Geometric Derivation of the Park Transformation

There are two versions of the Park transformation: the standard (amplitude-invariant) transformation and the power-invariant transformation. The derivation introduced by Park in Fig. 4(b) is the amplitude-invariant form, which is the most commonly used version. It is convenient because the magnitude of v_d is the same as the magnitude of v_a if two conditions are met: the voltages are balanced and the reference signal is in phase with phase a.

Previous approaches to deriving the Park transformation either use: trigonometric projection with coplanar abc axes [13] or modifying symmetrical components to obtain Clarke's matrix [11] and applying a rotation matrix. This section derives

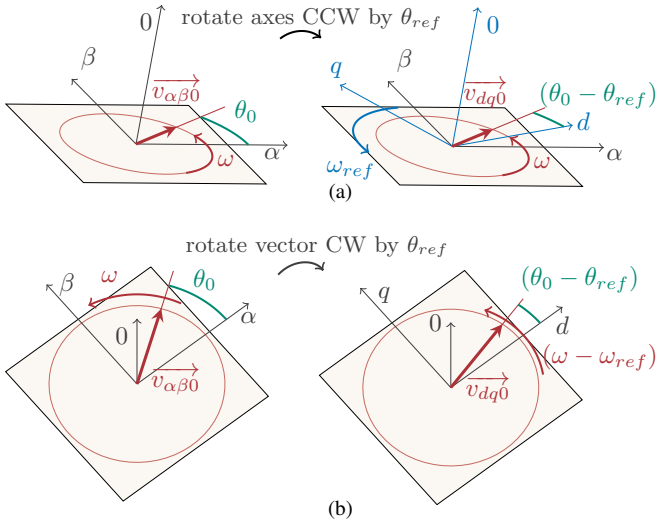

Fig. 12. The $\alpha\beta 0$ to $dq0$ transformation:
(a) Axes transformation perspective: rotate axes CCW about 0-axis by θ_{ref}.
(b) Vector transformation perspective: rotate vector CW about 0-axis by θ_{ref}.

the Park transformation matrix using the geometric approach. We utilise the relationship between the Park and Clarke transformations as shown in Fig. 1. The Park transformation can be decomposed into two consecutive transformations: the Clarke transformation followed by the $\alpha\beta 0$ to $dq0$ transformation. Section III details the geometric derivation of the Clarke transformation. This section completes the Park transformation matrix derivation by first deriving the $\alpha\beta 0$ to $dq0$ transformation. Then the Park transformation matrix is obtained by simple matrix multiplication. The overall geometric interpretation of the Park transformation is summarised in Fig. 5.

A. Transformation between Reference-Frames: $\alpha\beta 0$ to $dq0$ Transformation Derivation

The "transformation between reference-frames" or simply "frame-to-frame transformation" in [1] is used in multimachine [3] and multi-inverter modelling [4]. Each device is modelled in its own $dq0$ reference-frame, and each $dq0$ frame may have a different angle θ with respect to a common reference-frame. All devices can be translated to the common reference-frame using the transformation between two rotating $dq0$ frames [4]. The matrix describing this transformation has the same form as one that transforms from a stationary to a rotating $dq0$ reference-frame. The transformation between two rotating $dq0$ frames is equivalent to this paper's $\alpha\beta 0$ to $dq0$ transformation. We use Eq. (4) to derive this transformation, whereas the "transformation between reference-frames" is derived in an alternative manner, using matrix multiplication: see section 3.10 of [1].

The $\alpha\beta 0$ to $dq0$ transformation can be geometrically interpreted in $\mathbb{R}^3$ as a pure rotation about the 0-axis by a specified angle θ_{ref}. Fig. 12 illustrates the axes and vector transformation locus diagrams for the $\alpha\beta 0$ to $dq0$ transformation.

Fig. 12(a) is the axes transformation where the $\alpha\beta 0$ axes are rotated counterclockwise (CCW) about the 0-axis by an angle θ_{ref}. It is helpful to visualise the motion of the axes and vectors to understand the $\alpha\beta 0$ to $dq0$ transformation. Balanced systems have a Cartesian vector $\overrightarrow{v_{\alpha\beta 0}}$ that lies in the $\alpha\beta$-plane and rotates CCW about the 0-axis at speed ω. Note that $\overrightarrow{v_{\alpha\beta 0}}$ has an arbitrary angle θ_0 with respect to the α-axis ($\theta_0 = \omega t + \phi_0$). The $\alpha\beta 0$ axes are stationary and θ_0 increases with time.

The $dq0$ axes of Fig. 12(a) are not stationary, unlike the $\alpha\beta 0$ axes. These $dq0$ axes rotate CCW about the 0-axis at an angle $\theta_{ref} = \omega_{ref}\, t + \phi_{ref}$. $\overrightarrow{v_{dq0}}$ is the Cartesian vector referenced to $dq0$ coordinates. If $\omega_{ref} = \omega$ then $\overrightarrow{v_{dq0}}$ will have v_d and v_q components which appear constant as the $dq0$ axes are rotating at the same speed as the Cartesian vector $\overrightarrow{v_{dq0}}$. This case is illustrated by condition (i) of Fig. 2.

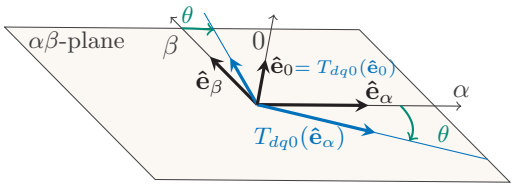

Fig. 13. Geometric $\alpha\beta 0$ to $dq0$ derivation :
(i) rotate $\hat{\mathbf{e}}_\alpha$ CW about 0-axis by θ_{ref}
(ii) rotate $\hat{\mathbf{e}}_\beta$ CW about 0-axis by θ_{ref} (iii) preserve $\hat{\mathbf{e}}_0$ under T_{dq0}.
Note: This figure uses the vector transformation perspective shown in Fig. 12(b). This perspective highlights that the unit vectors rotate CW. While the axis transformation perspective in Fig. 12(a) has a CCW rotation of axes.

Fig. 12(b) is the vector transformation, where the axes are fixed and the Cartesian vector $\overrightarrow{v_{\alpha\beta 0}}$ is rotated clockwise (CW) about the 0-axis by an angle θ_{ref}. Thus, the vector has a net CCW angle of $\theta_0 - \theta_{ref}$ relative to the d-axis. $\overrightarrow{v_{\alpha\beta 0}}$ is rotating CCW at an angular velocity ω when referenced to the $\alpha\beta 0$ axes. When referenced to the $dq0$ axes, the vector $\overrightarrow{v_{dq0}}$ has a CCW angular velocity of $\omega - \omega_{ref}$. If $\omega_{ref} = \omega$ then $\overrightarrow{v_{dq0}}$ will appear stationary on the $dq0$ axes.

$$\overrightarrow{v_{dq0}} = T_{dq0}\left(\overrightarrow{v_{\alpha\beta 0}}\right) = \boldsymbol{A_{dq0}}\overrightarrow{v_{\alpha\beta 0}} \tag{25}$$

The matrix $\boldsymbol{A_{dq0}}$ in Eq. (25) is found using Eq. (4). We apply T_{dq0} to each basis vector $\{\hat{\mathbf{e}}_\alpha, \hat{\mathbf{e}}_\beta, \hat{\mathbf{e}}_0\}$ as shown in Fig. 13. T_{dq0} rotates the vectors $\hat{\mathbf{e}}_\alpha$ and $\hat{\mathbf{e}}_\beta$ CW about the 0-axis by θ_{ref}. The components of $T_{dq0}(\hat{\mathbf{e}}_\alpha)$ and $T_{dq0}(\hat{\mathbf{e}}_\beta)$ can be found using trigonometric relations.

$$T_{dq0}(\hat{\mathbf{e}}_\alpha) = [\cos\theta \quad -\sin\theta \quad 0]^\intercal \tag{26}$$

$$T_{dq0}(\hat{\mathbf{e}}_\beta) = [\sin\theta \quad \cos\theta \quad 0]^\intercal \tag{27}$$

Fig. 13 shows how $\hat{\mathbf{e}}_0$ is preserved under T_{dq0}.

$$T_{dq0}(\hat{\mathbf{e}}_0) = \begin{bmatrix}0 & 0 & 1\end{bmatrix}^\intercal \tag{28}$$

The three transformed unit vectors given by Eq. (26), Eq. (27) and Eq. (28) are combined with Eq. (4) to find $\boldsymbol{A_{dq0}}$. The inverse transformation is found readily as the matrix is orthogonal ($\boldsymbol{A_{dq0}}^\intercal = \boldsymbol{A_{dq0}^{-1}}$).

$$\boldsymbol{A_{dq0}} = \begin{bmatrix} \cos\theta & \sin\theta & 0 \\ -\sin\theta & \cos\theta & 0 \\ 0 & 0 & 1 \end{bmatrix} \tag{29}$$

B. Power-Invariant Park Transformation Derivation

We derive Park's transformation utilising the relationships between the transformations in Fig. 1. The Park transformation is decomposed into the Clarke and $\alpha\beta 0$ to $dq0$ transformations in Eq. (30).

$$\overrightarrow{v_{dq0}} = T_{dq0}\left(T_c\left(\overrightarrow{v_{abc}}\right)\right) = \boldsymbol{A_{dq0}}\boldsymbol{A_c}\overrightarrow{v_{abc}} = \boldsymbol{A_p}\overrightarrow{v_{abc}} \tag{30}$$

The power-invariant Park transformation is constructed using the power-invariant Clarke transformation of Eq. (20) and the $\alpha\beta 0$ to $dq0$ transformation in Eq. (29). Please refer to Section III-A for a comprehensive derivation of the power-invariant Clarke transformation.

$$\boldsymbol{A_p} = \boldsymbol{A_{dq0}}\boldsymbol{A_c} = \boldsymbol{A_{dq0}}\sqrt{\frac{2}{3}}\begin{bmatrix} 1 & -\frac{1}{2} & -\frac{1}{2} \\ 0 & \frac{\sqrt{3}}{2} & -\frac{\sqrt{3}}{2} \\ \frac{1}{\sqrt{2}} & \frac{1}{\sqrt{2}} & \frac{1}{\sqrt{2}} \end{bmatrix}$$

$$\boldsymbol{A_p} = \sqrt{\frac{2}{3}}\begin{bmatrix} \cos\theta & \cos\left(\theta - \frac{2\pi}{3}\right) & \cos\left(\theta + \frac{2\pi}{3}\right) \\ -\sin\theta & -\sin\left(\theta - \frac{2\pi}{3}\right) & -\sin\left(\theta + \frac{2\pi}{3}\right) \\ \frac{1}{\sqrt{2}} & \frac{1}{\sqrt{2}} & \frac{1}{\sqrt{2}} \end{bmatrix} \tag{31}$$

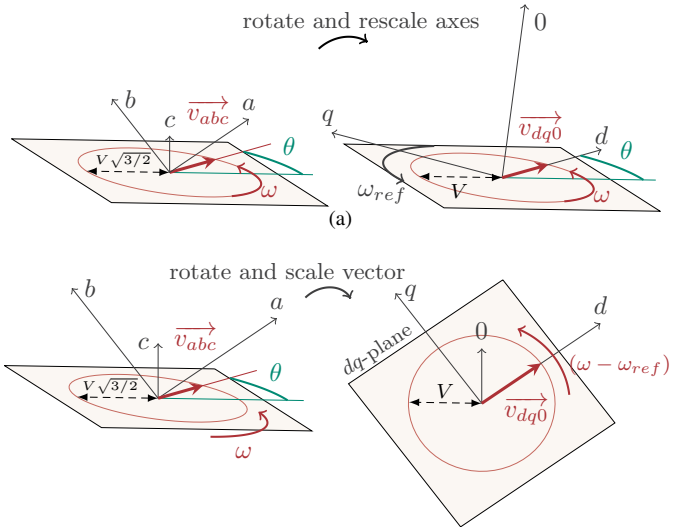

Fig. 14. The standard (amplitude-invariant) Park transformation:
(a) Axes transformation perspective: rotate the abc-axes such that the a-axis lines up with the vector v_{abc} at θ, and the b-axis also lies in the plane. Stretch the rotated ab-axes by $\sqrt{3/2}$ such that v_{dq0} has a length of V, when referenced to the dq-axes. The rotated and stretched ab-axes become our dq-axes respectively. The rotated c-axis becomes our 0-axis, and is stretched by $\sqrt{3}$ in order to agree with the definition of zero-sequence.
(b) Vector transformation perspective: rotate the vector v_{abc} such that it lies in the ab-plane, and it rotates CCW about the 0-axis at a speed $\omega - \omega_{ref}$. Scale the rotated v_{abc} by $\sqrt{2/3}$ such that it has a length of V when referenced to the dq-plane. The 0-component of the vector v_{dq0} is scaled by $1/\sqrt{3}$ in order to agree with the definition of zero-sequence.
Note: In both figures (a) and (b) the voltages are balanced, meaning the locus of v_{abc} is a circle of radius $V\sqrt{3/2}$.

C. Standard Park Transformation Derivation

The standard Park transformation can be determined in the same way as the power-invariant transformation using the relationships between the transformations (see Fig. 1) and Eq. (30). The difference is that we substitute the standard Clarke transformation of Eq. (24) for $\boldsymbol{A_c}$. $\boldsymbol{A_{dq0}}$ is given by Eq. (29). Please refer to Section III-B for a comprehensive derivation of the standard Clarke transformation.

$$\boldsymbol{A_p} = \boldsymbol{A_{dq0}}\boldsymbol{A_c} = \boldsymbol{A_{dq0}}\frac{2}{3}\begin{bmatrix} 1 & -\frac{1}{2} & -\frac{1}{2} \\ 0 & \frac{\sqrt{3}}{2} & -\frac{\sqrt{3}}{2} \\ \frac{1}{2} & \frac{1}{2} & \frac{1}{2} \end{bmatrix}$$

$$\boldsymbol{A_p} = \frac{2}{3}\begin{bmatrix} \cos\theta & \cos\left(\theta - \frac{2\pi}{3}\right) & \cos\left(\theta + \frac{2\pi}{3}\right) \\ -\sin\theta & -\sin\left(\theta - \frac{2\pi}{3}\right) & -\sin\left(\theta + \frac{2\pi}{3}\right) \\ \frac{1}{2} & \frac{1}{2} & \frac{1}{2} \end{bmatrix} \tag{32}$$

D. Standard Park Transformation Derivation: A Direct Geometric Approach

In this paper we decoupled the Park transformation into two operations, as shown in Fig. 5. Understanding the Park transformation as two consecutive operations highlights the geometric relationship between the Clarke, Park and frame-to-frame transformations.

Alternatively, one can use the geometric approach to directly derive the transformation from abc to $dq0$, without considering an intermediate $\alpha\beta0$ reference frame. In this section, we show this direct derivation for the standard Park transformation using the approach outlined in Section II-A and given by Eq. (4). The power-invariant Park transformation can also be found directly using a similar approach.

Fig. 14 illustrates the standard abc to $dq0$ transformation. This is plotted for the case where the d-axis lines up with the vector $\overrightarrow{v_{dq0}}$. Refer to Fig. 12 for the case where the d-axis may not be in line with $\overrightarrow{v_{dq0}}$. Fig. 14(a) shows the axis transformation, where we see the axes rotating and stretching so that $\overrightarrow{v_{dq0}}$ traces out a circle of radius V in the dq-plane.

Fig. 14(b) shows the same standard Park transformation from a different perspective. Instead of rotating and stretching the axes, we do the opposite. The axes are fixed and we rotate and scale the vector so that $\overrightarrow{v_{dq0}}$ has a length of V and moves CCW about the 0-axis at a net speed of $\omega - \omega_{ref}$ relative to the dq-axes. $\overrightarrow{v_{dq0}}$ will appear stationary relative to the dq-axes, if we apply Park's matrix using a reference signal at the same frequency as the phase voltages ($\omega_{ref} = \omega$).

The inverse Park transformation T_p^{-1} is more convenient to derive geometrically than T_p (analogous to why we derived T_c^{-1} in Section III). One can visualise how T_p^{-1} transforms vectors by reading Fig. 14 from right to left. The inverse transformation rotates the unit vectors $\hat{\mathbf{e}}_d$ and $\hat{\mathbf{e}}_q$ such that they lie in the plane of $\overrightarrow{v_{abc}}$. Thus, these transformed unit vectors $T_p^{-1}(\hat{\mathbf{e}}_d), T_p^{-1}(\hat{\mathbf{e}}_q)$ have a direction given by $\overrightarrow{v_{abc}}$ at angles of θ and $\theta + \pi/2$ respectively. Whereas T_p rotates the abc unit vectors $\hat{\mathbf{e}}_a, \hat{\mathbf{e}}_b, \hat{\mathbf{e}}_c$ to a location that is inconvenient to determine.

We derive Park's matrix by applying Eq. (4), which requires finding all three transformed unit vectors. These three steps are shown graphically by Fig. 15, where each of the unit vectors $\hat{\mathbf{e}}_d, \hat{\mathbf{e}}_q, \hat{\mathbf{e}}_0$ are transformed under T_p^{-1}. Fig. 15(a) shows how $\hat{\mathbf{e}}_d$ is transformed under the inverse Park transformation. $\hat{\mathbf{e}}_d$ is rotated such that it lines up with $\overrightarrow{v_{abc}}$ at angle θ and stretched by $\sqrt{3/2}$.

$$T_p^{-1}(\hat{\mathbf{e}}_d) = \overrightarrow{v_{abc}}\Big|_{\substack{V=1 \\ \theta}} = \begin{bmatrix} V\cos\theta \\ V\cos\left(\theta - \frac{2\pi}{3}\right) \\ V\cos\left(\theta + \frac{2\pi}{3}\right) \end{bmatrix}\Big|_{\substack{V=1 \\ \theta}}$$

$$T_p^{-1}(\hat{\mathbf{e}}_d) = \begin{bmatrix}\cos\theta & \cos\left(\theta - \frac{2\pi}{3}\right) & \cos\left(\theta + \frac{2\pi}{3}\right)\end{bmatrix}^\intercal \tag{33}$$

Similarly, Fig. 15(b) shows that $\hat{\mathbf{e}}_q$ is rotated and stretched by $\sqrt{3/2}$ such that it lines up with $\overrightarrow{v_{abc}}$ at angle $\theta + \pi/2$.

$$\begin{aligned} T_p^{-1}(\hat{\mathbf{e}}_q) &= \overrightarrow{v_{abc}}\Big|_{\substack{V=1 \\ \theta+\frac{\pi}{2}}} \\ &= \begin{bmatrix}\cos\left(\theta + \frac{\pi}{2}\right) & \cos\left(\theta + \frac{\pi}{2} - \frac{2\pi}{3}\right) & \cos\left(\theta + \frac{\pi}{2} + \frac{2\pi}{3}\right)\end{bmatrix}^\intercal \\ &= \begin{bmatrix}-\sin\left(\theta\right) & -\sin\left(\theta - \frac{2\pi}{3}\right) & -\sin\left(\theta + \frac{2\pi}{3}\right)\end{bmatrix}^\intercal \end{aligned} \tag{34}$$

Fig. 15(c) explains how $\hat{\mathbf{e}}_0$ is transformed. It points perpendicular to the plane of the locus and is scaled by $\sqrt{3}$, in order to correspond to the definition of zero-sequence. Mathematically, $T_p^{-1}(\hat{\mathbf{e}}_0) = [1 \quad 1 \quad 1]^\intercal$ is found by taking the cross-product of the other two transformed unit vectors, and scaled by $\sqrt{3}$, just as we saw in Eq. (23).

All three transformed unit vectors are combined using Eq. (4) ($\boldsymbol{A_p^{-1}} = [T_p^{-1}(\hat{\mathbf{e}}_d) \quad T_p^{-1}(\hat{\mathbf{e}}_q) \quad T_p^{-1}(\hat{\mathbf{e}}_0)]$) to give the standard inverse Park transformation matrix. We can take the inverse of Eq. (35) to obtain the transformation from abc to $dq0$, which will result in Eq. (32).

$$\boldsymbol{A_p^{-1}} = \begin{bmatrix} \cos\theta & -\sin\theta & 1 \\ \cos\left(\theta - \frac{2\pi}{3}\right) & -\sin\left(\theta - \frac{2\pi}{3}\right) & 1 \\ cos\left(\theta + \frac{2\pi}{3}\right) & -\sin\left(\theta + \frac{2\pi}{3}\right) & 1 \end{bmatrix} \tag{35}$$

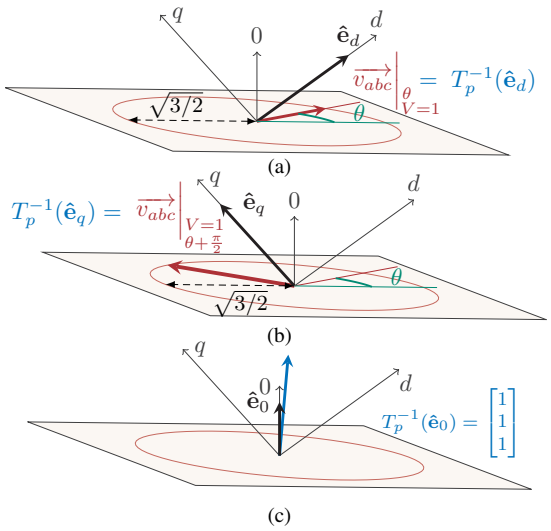

Fig. 15. Geometric standard (amplitude-invariant) inverse Park derivation: (a) rotate $\hat{\mathbf{e}}_d$ to align with the vector v_{abc} at θ and stretch by $\sqrt{3/2}$ (b) rotate $\hat{\mathbf{e}}_q$ to align with the vector v_{abc} at $\theta + \frac{\pi}{2}$ and stretch by $\sqrt{3/2}$ (c) rotate $\hat{\mathbf{e}}_0$ perpendicular to the plane and stretch by $\sqrt{3}$. Note: This figure has stationary $dq0$-axes, as it uses the vector transformation perspective shown in Fig. 14(b). This perspective highlights how the unit vectors stretch and rotate, which allows us to evaluate Eq. (4).

V. A Geometric Perspective on Power Quality

Power quality refers to harmonics and unbalance - both of which exist in all practical systems to some degree. Symmetrical components and the phasor representation are some of the tools used to analyse unbalanced systems. This section proposes an alternative view on power quality: a geometric interpretation. The locus diagram introduced in Section II-C is applied to three-phase quantities with harmonics or unbalanced phases.

A. Unbalance: A Geometric Perspective

Phasor diagrams are commonly used to represent unbalanced three-phase quantities. Fig. 16(a) shows an example system that contains positive, negative and zero-sequence components, similar to condition (ii) of Fig. 2.

The locus diagrams for the unbalanced system of Fig. 16(a) are presented in abc coordinates in Fig. 16(b). $\overrightarrow{v_{abc}}$ traces out an ellipse that lies outside the $\alpha\beta$-plane. This vector $\overrightarrow{v_{abc}}$ can be decomposed into three vectors corresponding to positive, negative and zero-sequence as shown in Fig. 16(b). The positive and negative sequence loci lie in the $\alpha\beta$-plane, although their vectors rotate in opposite directions. The zero-sequence locus is a line-segment perpendicular to the $\alpha\beta$-plane and is traced out by a pulsating zero vector.

Fig. 16(b) provides insights on how symmetrical components appear on locus diagrams. The locus of systems with purely positive and negative sequence will always lie in the $\alpha\beta$-plane. This can be shown by taking the span of the two vectors $\overrightarrow{v_{dq0_+}}$ and $\overrightarrow{v_{dq0_-}}$ which is always equal to the $\alpha\beta$-plane (assuming an instant in time where the vectors are not overlapping, in which case the span is a line). The locus of systems that contain zero-sequence will not lie in the $\alpha\beta$-plane.

Fig. 16(c) shows the locus diagrams of the unbalanced system in $dq0$ coordinates. In this example, we assume that the $dq0$ axes are rotating at the same speed ω as the signal. The positive sequence vector in $dq0$ coordinates rotates in the same direction as the $dq0$ axes. Therefore, positive sequence d and q-components will appear as constant values. The negative sequence vector rotates in the opposite direction as the dq axes, and its d and q-components will thus appear as a 2nd harmonic. Naturally, the zero-sequence component lies on the 0-axis.

B. Harmonics: A Geometric Perspective

Harmonics generate positive, negative and zero sequence components in an interesting pattern [30]. The positive sequence harmonics are 1st, 4th, 7th and so on. The harmonics 2nd, 5th and 8th etc appear as negative sequence. Triplen harmonics (3rd, 6th, 9th etc.) appear as zero-sequence in the abc domain. The first three harmonics are illustrated in Fig. 17(a).

The locus diagrams of Fig. 17(b) provide an intuitive means to understand how harmonics appear in $dq0$. The relative velocity of a vector and the $dq0$-axes determines what frequency a harmonic appears at. Positive sequence components rotate in the same direction as the $dq0$ axes. Thus, $\overrightarrow{v_{dq0_4}}$ and $\overrightarrow{v_{dq0_7}}$ have d and q-components containing the 3rd and 6th harmonics respectively. Negative sequence components appear faster relative to the $dq0$ axes, such that $\overrightarrow{v_{dq0_2}}$ and $\overrightarrow{v_{dq0_5}}$ have d and q-components with the 3rd and 6th harmonics respectively.

Finally, a single locus diagram can fully represent a signal containing harmonics. This is not possible with a phasor diagram. Fig. 18 shows an example similar to case (iii) of Fig. 2. The vector $\overrightarrow{v_{abc}}$ contains fundamental, 5th and 7th harmonics. Both harmonics appear as a 6th harmonic in $dq0$ as given by the shape of the locus of Fig. 18, which has 6 lobes.

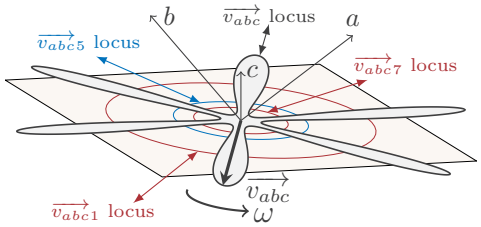

Fig. 18. Locus diagram of a 3-phase system with 1st, 5th and 7th harmonics.

VI. Conclusion

This paper develops a geometric approach to deriving the matrices describing the Clarke and Park transformations. The approach interprets each transformation as a combination of rotations and scalings in $\mathbb{R}^3$, and allows one to derive both the power-invariant and standard forms. The geometric perspective has applications in power quality. We show that, unlike the phasor diagram, a single locus diagram can fully represent a three-phase quantity with harmonics.

Appendix

A. Summary of Transformations and Instantaneous Power Calculations

Table I summarises the standard and power-invariant forms of the Clarke and Park transformations. Note that there are many conventions for the direction of the d and q axes, with some even having a q-axis lagging the d-axis. This paper follows the $dq0$ convention of Kundur and others in [21], [24] (see Table I). The angle θ is referenced with respect to the d-axis as shown in Fig. 4(a). There exists an alternative convention where the angle is referenced with respect to the q-axis. This convention ($qd0$) is used by Krause and others [1], [3].

Table II shows the instantaneous real and reactive power calculations in each of the $\alpha\beta0$ and $dq0$ domains. We use the definition of instantaneous reactive power given by [31].

Acknowledgment

The authors would like to acknowledge feedback from Sajjad Mohammadi, Mike Ranjram and Alex Hanson, graduate students at the Massachusetts Institute of Technology. We also would like to thank the editor and the anonymous reviewers for their constructive comments and suggestions regarding the contributions of this work. This research was supported by the Khalifa University of Science and Technology.

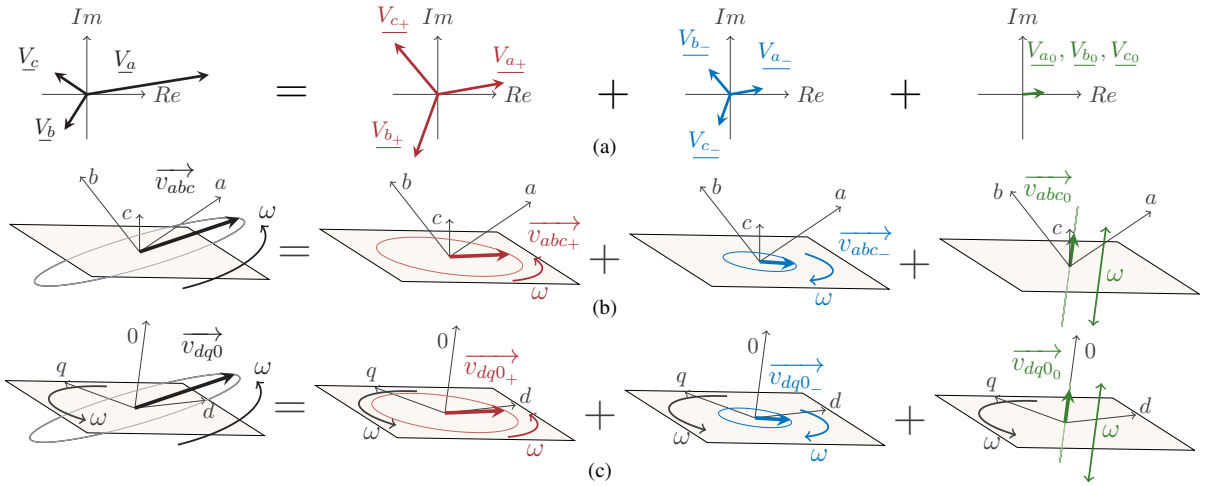

Fig. 16. Symmetrical components applied to an unbalanced 3-phase system with no harmonics. (a) phasor diagrams (b) locus diagrams in abc coordinates (c) locus diagrams in rotating $dq0$ coordinates.

TABLE I
SUMMARY OF TRANSFORMATIONS

	Standard (Amplitude-Invariant)	Power-Invariant
Clarke abc to $\alpha\beta 0$	$\frac{2}{3}\begin{bmatrix} 1 & -\frac{1}{2} & -\frac{1}{2} \\ 0 & \frac{\sqrt{3}}{2} & -\frac{\sqrt{3}}{2} \\ \frac{1}{2} & \frac{1}{2} & \frac{1}{2} \end{bmatrix}$	$\sqrt{\frac{2}{3}}\begin{bmatrix} 1 & -\frac{1}{2} & -\frac{1}{2} \\ 0 & \frac{\sqrt{3}}{2} & -\frac{\sqrt{3}}{2} \\ \frac{1}{\sqrt{2}} & \frac{1}{\sqrt{2}} & \frac{1}{\sqrt{2}} \end{bmatrix}$
Park abc to $dq0$	$\frac{2}{3}\begin{bmatrix} \cos(\theta) & \cos\left(\theta-\frac{2\pi}{3}\right) & \cos\left(\theta+\frac{2\pi}{3}\right) \\ -\sin(\theta) & -\sin\left(\theta-\frac{2\pi}{3}\right) & -\sin\left(\theta+\frac{2\pi}{3}\right) \\ \frac{1}{2} & \frac{1}{2} & \frac{1}{2} \end{bmatrix}$	$\sqrt{\frac{2}{3}}\begin{bmatrix} \cos(\theta) & \cos\left(\theta-\frac{2\pi}{3}\right) & \cos\left(\theta+\frac{2\pi}{3}\right) \\ -\sin(\theta) & -\sin\left(\theta-\frac{2\pi}{3}\right) & -\sin\left(\theta+\frac{2\pi}{3}\right) \\ \frac{1}{\sqrt{2}} & \frac{1}{\sqrt{2}} & \frac{1}{\sqrt{2}} \end{bmatrix}$
Inverse Clarke $\alpha\beta 0$ to abc	$\begin{bmatrix} 1 & 0 & 1 \\ -\frac{1}{2} & \frac{\sqrt{3}}{2} & 1 \\ -\frac{1}{2} & -\frac{\sqrt{3}}{2} & 1 \end{bmatrix}$	$\sqrt{\frac{2}{3}}\begin{bmatrix} 1 & 0 & \frac{1}{\sqrt{2}} \\ -\frac{1}{2} & \frac{\sqrt{3}}{2} & \frac{1}{\sqrt{2}} \\ -\frac{1}{2} & -\frac{\sqrt{3}}{2} & \frac{1}{\sqrt{2}} \end{bmatrix}$
Inverse Park $dq0$ to abc	$\begin{bmatrix} \cos(\theta) & -\sin(\theta) & 1 \\ \cos\left(\theta-\frac{2\pi}{3}\right) & -\sin\left(\theta-\frac{2\pi}{3}\right) & 1 \\ \cos\left(\theta+\frac{2\pi}{3}\right) & -\sin\left(\theta+\frac{2\pi}{3}\right) & 1 \end{bmatrix}$	$\sqrt{\frac{2}{3}}\begin{bmatrix} \cos(\theta) & -\sin(\theta) & \frac{1}{\sqrt{2}} \\ \cos\left(\theta-\frac{2\pi}{3}\right) & -\sin\left(\theta-\frac{2\pi}{3}\right) & \frac{1}{\sqrt{2}} \\ \cos\left(\theta+\frac{2\pi}{3}\right) & -\sin\left(\theta+\frac{2\pi}{3}\right) & \frac{1}{\sqrt{2}} \end{bmatrix}$

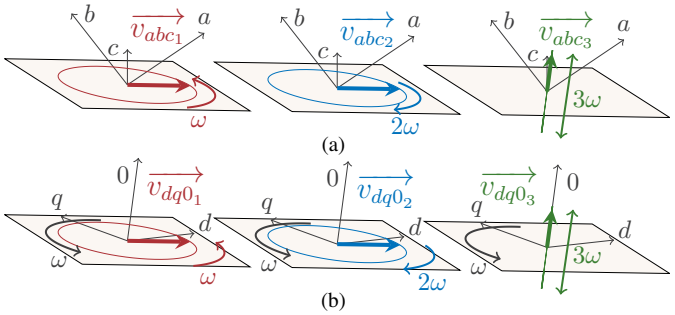

Fig. 17. Locus diagrams of first three harmonics in: (a) abc coordinates (b) $dq0$ coordinates.

TABLE II
SUMMARY OF INSTANTANEOUS POWER CALCULATIONS

	Standard (Amplitude-Invariant)	Power-Invariant
$\alpha\beta 0$	$p(t) = \frac{3}{2}\left(v_\alpha i_\alpha + v_\beta i_\beta + 2v_0 i_0\right)$	$p(t) = v_\alpha i_\alpha + v_\beta i_\beta + v_0 i_0$
	$q(t) = \frac{3}{2}\left(v_\beta i_\alpha - v_\alpha i_\beta\right)$	$q(t) = v_\beta i_\alpha - v_\alpha i_\beta$
$dq0$	$p(t) = \frac{3}{2}\left(v_d i_d + v_q i_q + 2v_0 i_0\right)$	$p(t) = v_d i_d + v_q i_q + v_0 i_0$
	$q(t) = \frac{3}{2}\left(v_q i_d - v_d i_q\right)$	$q(t) = v_q i_d - v_d i_q$

REFERENCES

[1] P. Krause, O. Wasynczuk, S. D. Sudhoff, and S. Pekarek, *Analysis of electric machinery and drive systems*. John Wiley & Sons, 2013.

[2] B. K. Bose, *Modern power electronics and AC drives*. Prentice Hall, 2002.

[3] P. W. Sauer and M. A. Pai, *Power system dynamics and stability*. Wiley-IEEE Press, 1998.

[4] N. Pogaku, M. Prodanovic, and T. C. Green, "Modeling, analysis and testing of autonomous operation of an inverter-based microgrid," *IEEE Transactions on power electronics*, vol. 22, no. 2, pp. 613–625, 2007.

[5] D. Baimel, J. Belikov, J. M. Guerrero, and Y. Levron, "Dynamic modeling of networks, microgrids, and renewable sources in the dq0 reference frame: A survey," *IEEE Access*, vol. 5, pp. 21 323–21 335, 2017.

[6] A. Aderibole, H. H. Zeineldin, M. S. El-Moursi, J. C.-H. Peng, and M. Al Hosani, "Domain of stability characterization for hybrid microgrids considering different power sharing conditions," *IEEE Transactions on Energy Conversion*, vol. 33, no. 1, pp. 312–323, 2018.

[7] J. A. Mueller and J. W. Kimball, "An efficient method of determining operating points of droop-controlled microgrids," *IEEE Transactions on Energy Conversion*, vol. 32, no. 4, pp. 1432–1446, 2017.

[8] N. Kroutikova, C. Hernandez-Aramburo, and T. C. Green, "State-space model of grid-connected inverters under current control mode," *IET Electric Power Applications*, vol. 1, no. 3, pp. 329–338, 2007.

[9] P. Mattavelli, "A closed-loop selective harmonic compensation for active

filters," *IEEE Transactions on Industry Applications*, vol. 37, no. 1, pp. 81–89, 2001.

[10] E. Clarke, "Determination of voltages and currents during unbalanced faults," *General Electric Review*, vol. 40, no. 11, pp. 511–513, 1937.

[11] ——, "Problems solved by modified symmetrical components," *General Electric Review*, vol. 41, no. 11 and 12, pp. 488–449, 1938.

[12] ——, *Circuit analysis of AC power systems*. Wiley, 1943, vol. 1.

[13] R. H. Park, "Two-reaction theory of synchronous machines generalized method of analysis-part I," *Transactions of the American Institute of Electrical Engineers*, vol. 48, no. 3, pp. 716–727, 1929.

[14] A. Blondel, "On the empirical theory of alternators," *L'Industrie Electrique*, 1899.

[15] A. Blondel and C. A. Adams, *Synchronous motors and converters: theory and methods of calculation and testing*. McGraw-Hill Book Company, 1913.

[16] R. Doherty and C. Nickle, "Synchronous machines I-an extension of blondel's two-reaction theory," *Transactions of the American Institute of Electrical Engineers*, vol. 45, pp. 912–947, 1926.

[17] H. C. Stanley, "An analysis of the induction machine," *Electrical Engineering*, vol. 57, no. 12, pp. 751–757, 1938.

[18] G. Kron, *Equivalent circuits of electric machinery*. J. Wiley & Sons, 1951.

[19] D. S. Brereton, D. G. Lewis, and C. G. Young, "Representation of induction-motor loads during power-system stability studies," *AIEE Trans. on PAS*, pp. 451–460, 1957.

[20] P. C. Krause and C. Thomas, "Simulation of symmetrical induction machinery," *IEEE transactions on power apparatus and systems*, vol. 84, no. 11, pp. 1038–1053, 1965.

[21] P. Kundur, N. J. Balu, and M. G. Lauby, *Power system stability and control*. McGraw-hill New York, 1994, vol. 7.

[22] P. C. Krause, F. Nozari, T. Skvarenina, and D. Olive, "The theory of neglecting stator transients," *IEEE Transactions on Power Apparatus and Systems*, no. 1, pp. 141–148, 1979.

[23] C. Concordia, *Synchronous machines: theory and performance*. Wiley, 1951.

[24] A. E. Fitzgerald, C. Kingsley, and S. D. Umans, *Electric machinery*. McGraw-Hill New York, 2003, vol. 5.

[25] T. Lipo, *A Cartesian vector approach to reference frame theory of AC machines*. Department of Electrical and Computer Engineering, University of Wisconsin-Madison, 1984.

[26] R. Zhang, V. H. Prasad, D. Boroyevich, and F. C. Lee, "Three-dimensional space vector modulation for four-leg voltage-source converters," *IEEE Transactions on power electronics*, vol. 17, no. 3, pp. 314–326, 2002.

[27] S. Gataric, "A polyphase cartesian vector approach to control of polyphase ac machines," in *Industry Applications Conference, 2000. Conference Record of the 2000 IEEE*, vol. 3. IEEE, 2000, pp. 1648–1654.

[28] A. A. Montanari and A. M. Gole, "Enhanced instantaneous power theory for control of grid connected voltage sourced converters under unbalanced conditions," *IEEE Transactions on Power Electronics*, vol. 32, no. 8, pp. 6652–6660, 8 2017.

[29] G. Strang, *Introduction to linear algebra*. Wellesley-Cambridge Press Wellesley, MA, 1993, vol. 3.

[30] P. Kanjiya, V. Khadkikar, and M. S. El Moursi, "A novel type-1 frequency-locked loop for fast detection of frequency and phase with improved stability margins," *IEEE Transactions on Power Electronics*, vol. 31, no. 3, pp. 2550–2561, 2016.

[31] H. Akagi, E. H. Watanabe, and M. Aredes, *Instantaneous power theory and applications to power conditioning*. John Wiley & Sons, 2017, vol. 62.

Colm J. O'Rourke (S'15) received the B.Eng. degree in energy systems engineering from the National University of Ireland, Galway, in 2013, and the S.M. degree in electrical engineering and computer science in 2015 from the Massachusetts Institute of Technology, Cambridge, MA, USA, where he is currently working toward the Ph.D. degree.

He was the lead Electrical Engineer on the 2017 MIT Hyperloop team. He has previously interned at Analog Devices, ESB International and Tesla Inc. in Palo Alto, California. His research interests include renewable energy integration, power system modelling, stability analysis and machine learning applications in power systems.

Mohammad M. Qasim (S'10) received the B.S. degree in electrical engineering from the American University of Sharjah, Sharjah, UAE and S.M. degree in electrical power engineering from the Masdar Institute of Science and Technology (MI), Abu Dhabi, UAE, in 2011 and 2013, respectively. From 2013 to 2015 he was a Research Engineer in the Laboratory of Electrical Power Engineering, MI. In 2015, he started graduate school at the Massachusetts Institute of Technology (MIT), Cambridge, MA, USA. He received the S.M. degree in electrical engineering and computer science from MIT in 2019. He is currently working toward the Ph.D. degree in the laboratory of Electromagnetic and Electronic Systems, MIT.

In the summer of 2018, he interned with the power electronics and control team at Tesla Inc., Palo Alto, CA, USA, where he worked on dc bus balancing of multilevel converters. His research interests include the design and control of electric machines and motor drives.

Matthew R. Overlin (S'19) received his B.S. and M. Eng. degrees in 2013 and 2017, respectively, in electrical engineering from the Massachusetts Institute of Technology. He is currently pursuing the Ph.D. degree in electrical engineering from the Massachusetts Institute of Technology. His research interests include power systems modeling and simulation, system identification, and numerical simulation. He applies numerical techniques to time-domain simulations in the area of power systems. He is a research assistant at the Massachusetts Institute of Technology Lincoln Laboratory in the Energy Systems Group where he models power flow and transient stability in microgrids.

James L. Kirtley (S'69–M'71–SM'80–F'91–LF'11) received the undergraduate and the Ph.D. degree from MIT, Cambridge, MA, USA, in 1971. He is currently a Professor with the Electrical Engineering Department, Massachusetts Institute of Technology. He was with General Electric, Large Steam Turbine Generator Department, as an Electrical Engineer, for Satcon Technology Corporation as a Vice President and a General Manager with the Tech Center, as a Chief Scientist, and as a Director. He was a Gastdozent with the Swiss Federal Institute of Technology, Zrich (ETH). He is a Specialist in electric machinery and electric power systems. He served as Editor-in-Chief of the IEEE TRANSACTIONS ON ENERGY CONVERSION from 1998 to 2006. He was the recipient of the IEEE Third Millennium Medal in 2000 and the Nikola Tesla Prize in 2002. He was elected to the United States National Academy of Engineering in 2007. He is a Registered Professional Engineer in Massachusetts.